Nuclear Engineering and Technology 55 (2023) 4048–4056

Contents lists available at ScienceDirect

Nuclear Engineering and Technology

journal homepage: www.elsevier.com/locate/net

Original Article

Coupled neutronics/thermal-hydraulic analysis of ANTS-100e using MCS/RAST-F two-step code system

Tung Dong Cao Nguyen, Tuan Quoc Tran, Deokjung Lee *

Department of Nuclear Engineering, Ulsan National Institute of Science and Technology, 50 UNIST-gil, Ulju-gun, Ulsan, 44919, Republic of Korea

ARTICLE INFO

Keywords:
MCS
RAST-F
Cross-section
LFR
ANTS-100e
Thermal-hydraulic

ABSTRACT

The feasibility of using the Monte Carlo code MCS to generate multigroup cross sections for nodal diffusion simulations RAST-F of liquid metal fast reactors is investigated in this paper. The performance of the MCS/RAST-F code system is assessed using steady-state simulations of the ANTS-100e core. The results show good agreement between MCS/RAST-F and MCS reference solutions, with a k_{eff} difference of less than 77 pcm and root-mean-square differences in radial and axial power of less than 0.5% and 0.25%, respectively. Furthermore, the MCS/RAST-F reactivity feedback coefficients are within three standard deviations of the MCS coefficients. To validate the internal thermal-hydraulic (TH) feedback capability in RAST-F code, the coupled neutronic/TH1D simulation of ANTS-100e is performed using the case matrix obtained from MCS branch calculations. The results are compared to those obtained using the MARS-LBE system code and show good agreement with relative temperature differences in fuel and coolant of less than 0.8%. This study demonstrates that the MCS/RAST-F code system can produce accurate results for core steady-state neutronic calculations and for coupled neutronic/TH simulations.

1. Introduction

Liquid metal-cooled fast reactors (LMFRs) have been a promising candidate for meeting future energy demands because of their high thermal efficiency and the potential for using nuclear waste as fuel. Their design and optimization, however, require a thorough understanding of the complex interplay between neutronics and thermal hydraulics (TH). Neutronic simulation coupled with TH feedback is a powerful tool to investigate the behavior of these reactors. This can aid in reactor design and optimization, which are essential for the advancement of safe and efficient nuclear power technologies. Several research studies have been conducted to develop simulation capabilities for LMFRs using various codes and methodologies. A study by Fridman et al. has presented the extension of the simulation capabilities of DYN3D from the sodium fast reactor (SFR) core to the system level by coupling DYN3D with a TH system code, ATHLET, that could perform sodium flow modeling [1]. Another research by Dawn and Palmtag has developed a multiphysics simulation suite for LMFRs, LUPINE, to model the Advanced Burner Reactor (ABR) MET-1000 benchmark with coupled neutronics, TH, and thermal expansion models [2]. Lindley et al. have investigated the coupling effect on the power distribution of SFRs using several state-of-the-art reactor physics and multiphysics codes to improve confidence in the methodologies and validity of the results [3]. In addition, Vazquez et al. have outlined the establishment of a coupled neutronics/TH code system using the Monte Carlo (MC) code MCNPX and the sub-channel code COBRA-IV, which is applied to an SFR concept at both the assembly and full core scales [4]. Fang et al. have introduced the neutronics/TH coupling analysis for a small lead-based FR using the discrete ordinate nodal and parallel channel method [5].

Motivated by the previous research, this paper presents a new two-step code system for neutronic simulation coupled with TH feedback from LMFRs. The MCS/RAST-F code system is based on the MC code MCS for generating multigroup cross-section (MG XS) data [6,7] and the nodal diffusion code RAST-F (RF) with an internal TH solver, TH1D [8,9]. The MCS/RF code system is validated first against the standalone MCS calculation for the lead-bismuth-cooled FR designs, ANST-100e, in a variety of neutronic parameters of interest, including core multiplication, power profiles, and reactivity coefficients. Second, a neutronic simulation with TH1D feedback is performed and compared to the MARS-LBE solution using the ANTS-100e as a reference core configuration.

This paper is structured as follows: Section 2 describes the ANTS-

* Corresponding author.
E-mail addresses: tungnguyen@unist.ac.kr (T.D.C. Nguyen), trantuan@unist.ac.kr (T.Q. Tran), deokjung@unist.ac.kr (D. Lee).

https://doi.org/10.1016/j.net.2023.07.020
Received 5 May 2023; Received in revised form 4 July 2023; Accepted 17 July 2023
Available online 20 July 2023

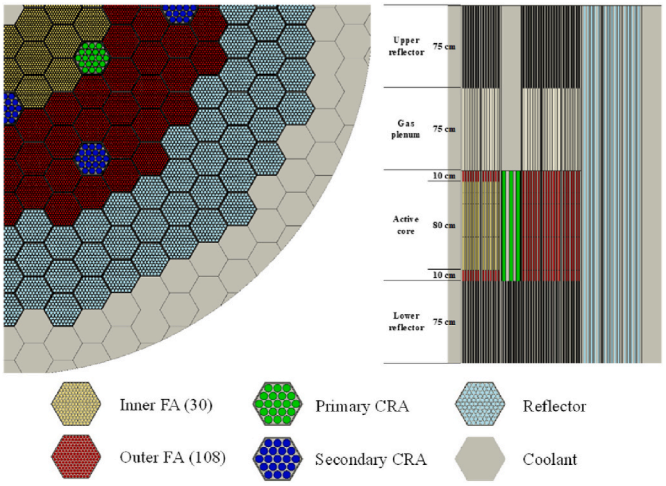

Fig. 1. Radial and axial layouts of the ANTS-100e quarter core.

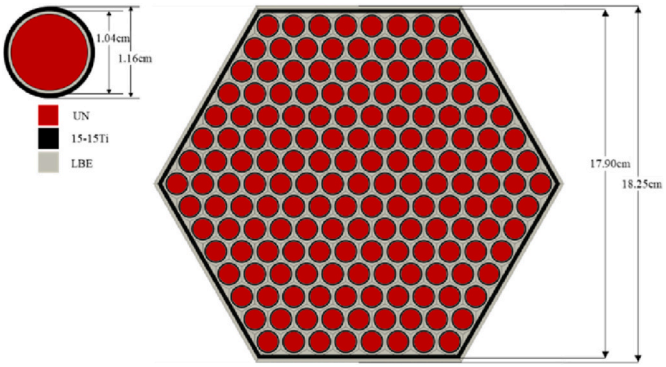

Fig. 2. Fuel pin and assembly design for ANTS-100e.

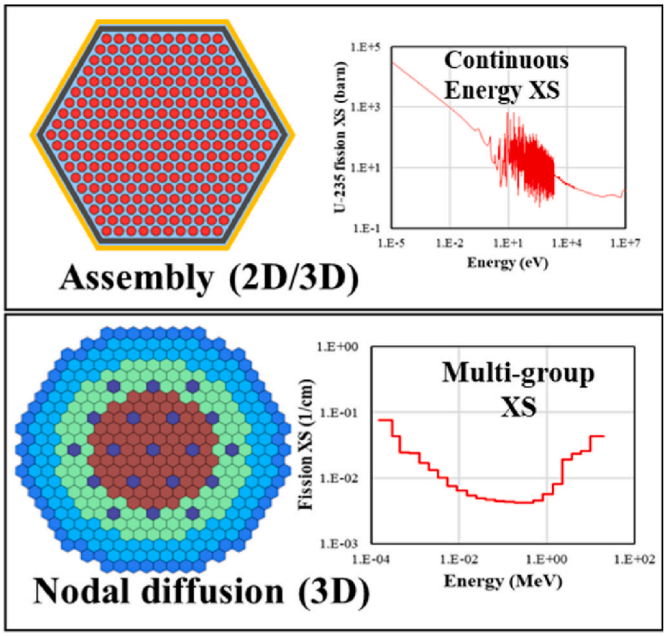

Fig. 3. Typical computation procedure for coarse-mesh FR whole-core calculation.

100e cores. Section 3 briefly introduces the MCS approach for tallying the MG XSs and the RF nodal diffusion code. Section 4 demonstrates a code-to-code comparison of the two-step code MCS/RF and the stand-alone MCS code against the steady-state simulation. Section 4 also discusses the verification of the neutronic simulation coupled with TH1D. Section 5 finally discusses the conclusions and future prospects.

2. Reactor core description

The ANTS-100e is a promising nuclear reactor design that can generate clean and sustainable energy over a 10-year first cycle. Fig. 1 [10] depicts the design layouts of the ANTS-100e core, which includes several unique features that make it a highly efficient and safe design. The active core is composed of 138 fuel assemblies (FAs), which are divided into two enrichment zones of 10.0% and 13.0% uranium nitride. The ANTS-100e core adopts onion core zoning, which results in axial enrichment zoning in the inner core: 13.0% enrichment at the top and bottom 10-cm and 10.0% enrichment in the middle. The use of uranium nitride as the fuel material results in higher thermal conductivity and uranium density, resulting in a higher fuel burnup and a more efficient use of fuel. The FAs are arranged in a hexagonal lattice configuration, as shown in Fig. 2, which allows for more uniform power distribution and better utilization of the available space. Lead-bismuth eutectic (LBE) is selected as coolant, and 15-15Ti stabilized steel is selected as cladding and duct materials for ANTS-100e. LBE is filled as a bond material between fuel pellets and cladding to reduce fuel centerline temperature.

Each fuel assembly consists of four axial components: the lower reflector, fuel, gas plenum, and upper reflector. The axial reflectors are made of stainless steel and are 75 cm long, providing an additional source of neutron moderation and reducing neutron leakage from the core. The gas plenum is also 75 cm long, which could be beneficial to compensate for the fission gas release in ANTS-100e. The use of a gas plenum also aids in the removal of the fission gases, reducing the buildup of pressure in the fuel rods and extending their lifespan.

The ANTS-100e core design includes two independent control rod systems: a primary system and a secondary system with three and nine control assemblies, respectively. The layout of each control rod assembly (CRA) is the same for both systems, with boron carbide as the primary absorber material (B_4C). The CRAs are designed to provide rapid and reliable control of the reactor power and to mitigate the consequences of any abnormal events. The flow rates are regulated by orifices attached at the bottom of the core.

The active core has an equivalent size of 235 cm in diameter and 100 cm in height, resulting in a height-to-diameter ratio of 0.43. This design feature ensures a low core power density and high reactor stability, preventing any critical accidents from occurring. The core design of the ANTS-100e can provide high fuel burnup, low core power density, and high reactor stability. This design is highly suitable for long-term, sustainable nuclear energy production with increased efficiency and reduced waste production.

3. MCS/RF two-step code system

3.1. Computer codes

MCS is a 3D continuous-energy neutron physics code for particle transport that has been in development since 2013 by the Ulsan National Institute of Science and Technology (UNIST) [11]. MCS can perform criticality and fixed source-runs for reactivity calculations and shielding problems, respectively. The neutron transport capability of MCS has been validated and verified using a variety of benchmark problems [12–15].

UNIST has also engaged in RAST-K code development for the diffusion core simulator [8,16]. It solves steady-state and transient problems with assembly-level nodes using the 3D nodal method and the MG coarse mesh finite difference acceleration technique. The triangular

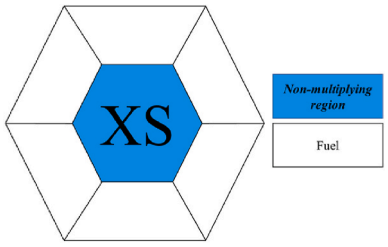

Fig. 4. 2D supercell model ("XS" indicates region where XSs are generated).

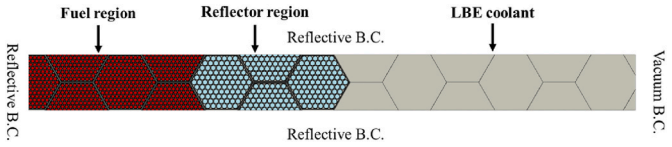

Fig. 5. Radial reflector model.

Table 1
Summary of branch conditions for ANTS-100e.

Branch	Fuel temperature (K)	Coolant temperature (K)	Coolant density (g/cm^3)
1	500	500	10.434
2	500	648	10.238
3	500	800	10.037
4	750	500	10.434
5	750	648	10.238
6	750	800	10.037
7	1,000	500	10.434
8	1,000	648	10.238
9	1,000	800	10.037

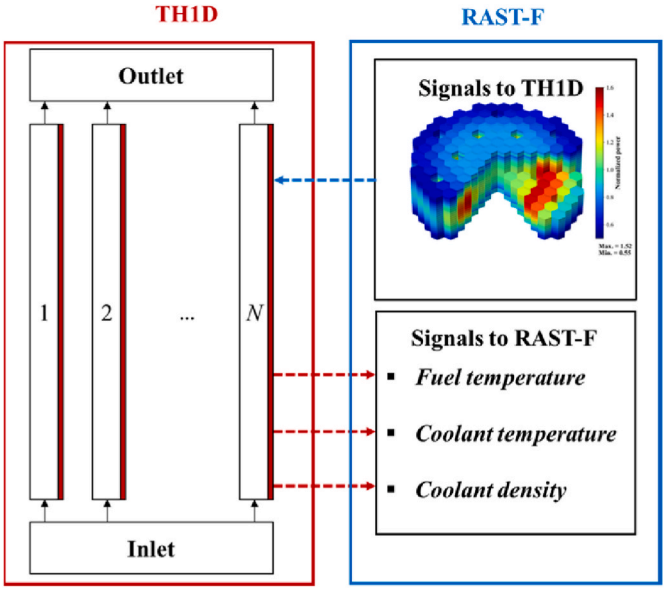

Fig. 6. RAST-F/TH1D internal coupling scheme.

polynomial expansion nodal method for FR analysis was recently implemented in RAST-K, and its version is known as RAST-F (RF) [9].

3.2. MCS/RF two-step code approach

Fig. 3 depicts a typical computation procedure for nodal FR whole-core analysis. The first step is to use MCS to generate a homogenized XS data library, which offers more modeling flexibility than traditional deterministic lattice transport codes. The homogenized XS data library is generated by simulating neutron transport processes in the representative unit cell of core components. The generated MG XS is then used to run RF nodal diffusion simulations, in which RF divides the core into several control volumes (nodal regions) and calculates the neutron flux and power distribution within each control volume using the nodal diffusion equations. If necessary, RF considers feedback effects such as TH and fuel depletion. The TH feedback scheme is described in the following section.

The 24-group energy structure was used in this work, which is a subset of the ECCO 33-group structure [17,18]. Because the MC method produces significant statistical uncertainties in neutron flux for the last ten groups of the ECCO-33, the 24-group structure is formed by combining the last ten thermal energy groups into a group. A standard approach for obtaining the 24-group XSs for each fast reactor component is outlined [7,17,18]. First, the FA XSs are calculated using a single 2D FA model with reflective boundary conditions (BCs). Second, the 2D supercell models are used to score the homogenized XS for non-multiplying zones such as CRA and axial components located far away from the active core, as shown in Fig. 4. To properly account for neutron leakage, the XS for the radial reflector assembly and its nearby FA is generated using the radial reflector model (RRM), as shown in Fig. 5, with the vacuum BC applied on the model's right side. A detailed analysis of the spectrum comparison of the radial reflector corresponding to the use of supercell and RRM is provided in ref. [7]. Finally, the 3D FA is used to generate the XS for axial components adjacent to the active core (i.e., lower reflector and gas plenum) to account for axial leakage. More detailed analysis on the XS generation can be found in ref. [7] including the XS models for correctly treating the axial and radial leakage, i.e., gas plenum and axial reflector regions. Furthermore, the super homogenization (SPH) method [19] is employed to modify the flux-volume-weighted XS of the prominently absorbing zone and its surroundings, i.e., the CRA and its six neighboring FAs.

3.3. MCS branch calculation

The MC code, MCS, offers an automated burnup sequence for executing branch variations. These variations in the TH state can be attributed to changes in material temperatures and densities, and if required, the burnup card for each branch can be enabled to generate the burnup dependent XSs. The MG XS library is parametrized in this study taking into account the fuel and coolant temperatures. However, it should be noted that axial fuel rod expansion and radial diagrid expansion are not taken into account in this work. These effects can also have an impact on the TH state of the reactor and should be considered in future studies.

The range of state parameters is selected to cover the entire range of reactor conditions. The variation in coolant temperature implicitly accounted for the variation in coolant density. Table 1 summarizes the variations in the branch cases for ANTS-100e. A total of 9 branch calculations are performed for each FA type. Notably, MCS can use the two nearest temperature points to perform XS interpolation for a temperature point that is not available in ENDF ACE files.

3.4. RAST-F internal thermal-hydraulic feedback TH1D

For TH feedback, the TH1D solver is implemented in RF, and the brief procedure is shown in Fig. 6. The neutronics code and the TH solver are independent in this framework, but they exchange variables that are input parameters for each code. The nodal power distribution is computed by the RF nodal diffusion code and passed to the TH1D solver. The data transferred from TH1D to RF includes node-wise distributions of TH properties such as fuel temperature, coolant temperature, and density. RAST-F uses these TH distributions to update the node-wise MG XSs, accounting for TH reactivity feedback. The process is iteratively

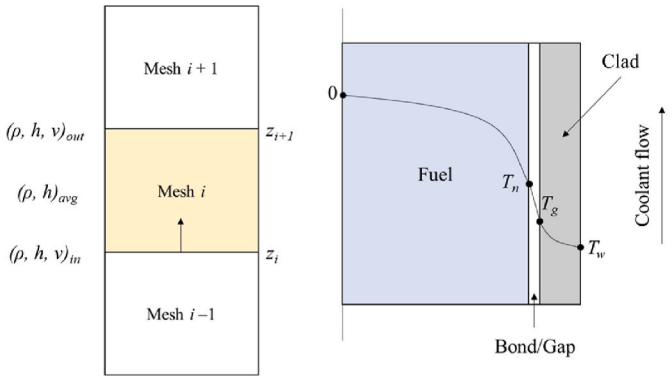

Fig. 7. Single channel TH1D solver axial (left) and radial (right) diagram.

Table 2
ANTS-100e core parameters, MCS/RF vs. MCS.

Parameter	MCS ($\pm 3\sigma$)	MCS/RF	Diff. ($\pm 3\sigma$, %)
k_{eff}	1.00861 ± 0.00007	1.00940	0.077 ± 0.007
FTC (pcm/K)	−1.338 ± 0.069	−1.334	−0.2 ± 5.2
CTC (pcm/K)	−0.186 ± 0.048	−0.180	−3.7 ± 25.7

repeated until certain convergence criteria are satisfied. The following is the program algorithm:

i. Executes the RF nodal diffusion calculation.
ii. Forwards power distribution to the TH1D solver.
iii. Solve TH equation with given RF power distribution.
iv. Fuel temperature-based convergence check.
v. Updates the TH conditions, including fuel temperature, coolant temperature, and coolant density, unless converged.
vi. Repeat steps i-iv until convergence is achieved.

It is important to note that in this coupling system, each FA is treated as a single TH channel, with RF coarse meshes determining the axial mesh size in TH1D. Because most fast reactor assemblies are enclosed by ducts, 1D flow is an acceptable presumption with no channel crossflow and ideal fluid mixing within each channel. TH1D solves two 1D equations radially and axially as shown in Fig. 7. To estimate coolant temperatures throughout each flow channel, a 1D axial heat convection model is established based on solving steady state mass and energy conservation equations, from which the channel-wise flow rate distribution can be fed into the RF by following the cooling groups or zones that are set up to flatten the outlet fuel and coolant temperatures. To obtain fuel temperatures in each hexagonal assembly and at each axial mesh, a 1D radial heat conduction model is established. For evaluating the fuel centerline temperature, the fuel zone is divided into ten rings. The convergence criterion is checked by comparing the temperature of current iteration i to the temperature of previous iteration $i-1$ as in Eq. (1),

$$\frac{T_i}{T_{i-1}} - 1 < \varepsilon, \tag{1}$$

where ε is the convergence criterion, which can be set by users and is 10^{-3} in this study. In general, the temperature will be converged after a few iterations. Detailed description of the TH1D solver can be found in ref. [20].

All the thermophysical properties of materials for TH1D are collected in ref. [21]. The equations for the TH properties of LBE used in RF can be found [22,23], in which many different models for LBE flow in rod bundles are listed. In this work, the Calamai et al. model [24] is selected, in which the Nusselt (Nu) correlation in Eq. (2) is valid with a pitch-to-diameter (P/D) ratio ranging from 1.1 to 1.4 and a Peclet number (Pe) ranging from 10 to 5,000. This correlation can be feasible for ANTS-100e because the P/D ratio is 1.15.

$$Nu = 4 + 0.16(P/D)^5 + 0.33(P/D)^{3.8}(Pe/100)^{0.86}. \tag{2}$$

Another significant variable for the TH1D solver is the energy deposition in the LBE coolant, which was found to be approximately 4% of the total deposited energy [25]. In RF, the TH1D solver employs a constant gap conductance determined by gap width and gap material, which in this case is an LBE bond. Users can enter these two variables into RF based on the given reactor coolant and design gap or bond material.

4. Results and discussions

4.1. Steady-state simulation results

In this study, the two-step code MCS/RF is verified against the reference solution, the MC code MCS, for several parameters of interest, including the core multiplication factor, fuel temperature coefficient (FTC), coolant temperature coefficient (CTC), and power profiled with all rods out (ARO). The reactivity coefficients FTC and CTC are calculated by subtracting the reactivity from two calculations and dividing by the change in the system parameter, which in this work is temperature and LBE density, respectively [26].

The ENDF/B-VII.0 library is used in all MCS simulations. As a reference, the MCS whole-core calculation is performed with 5 inactive batches, 40 active batches, and 8,000,000 particles per batch, with the

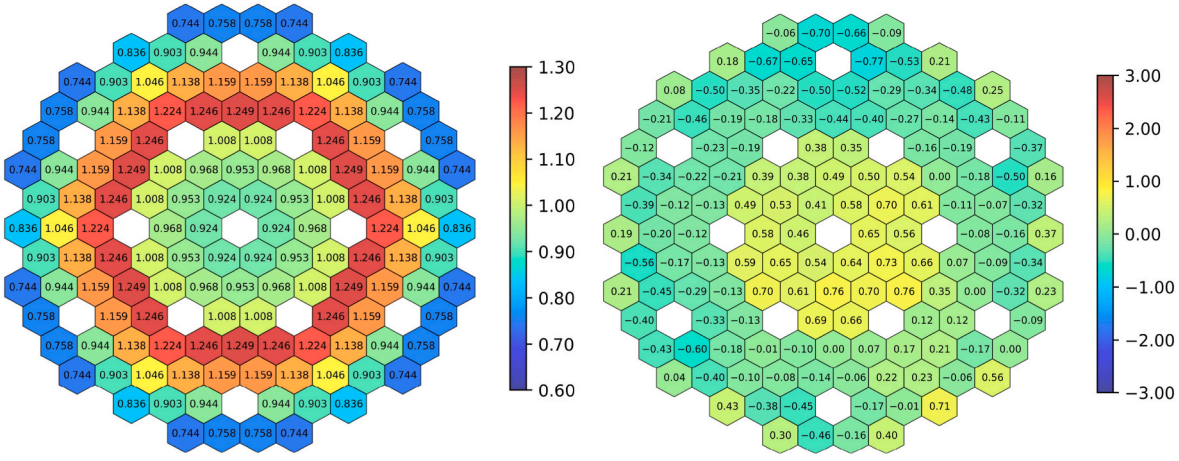

Fig. 8. Normalized radial assembly-wise power distribution by MCS/RF (left) and its difference to MCS (right).

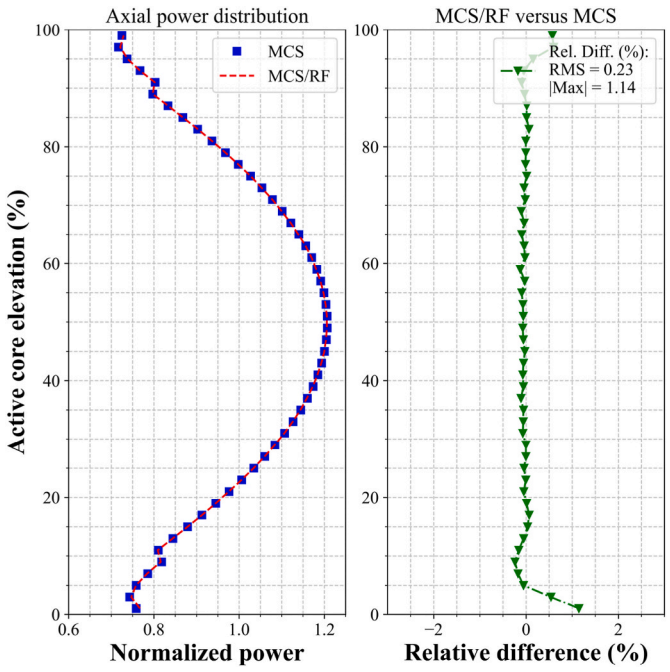

Fig. 9. Normalized axial power distribution, MCS/RF vs. MCS.

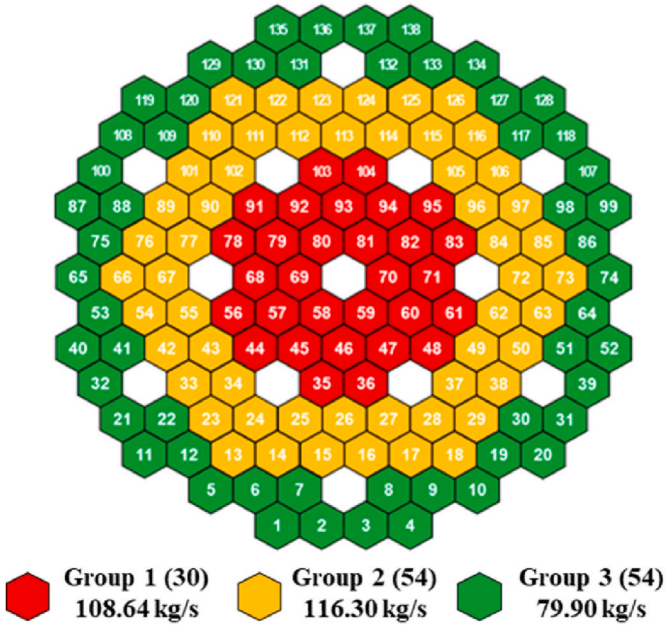

Fig. 10. Flow zones in ANTS-100e.

Table 3
Summary of relative power differences, MCS/R2 vs. MCS.

Rel. diff. (%)	|Max.|	RMS
Radial	0.77	0.39
Axial	1.14	0.23

Table 4
Summary of CRWs, MCS/RF vs. MCS.

Code		CRW (pcm)	Rel. diff. (%)
MCS (±3σ)		9,183 ± 21	–
MCS/RF	Without SPH	9,716	5.8
	With SPH (only CRA)	9,362	2.0
	With SPH (CRA + FAs)	9,158	−0.2

MCS relative standard deviation (SD) in radial and axial power being less than 0.25% and 0.1%, respectively. Because of the nature of the MC method, even with a large number of histories, the radial power cannot be completely symmetric.

The following equations are useful when conducting a code-to-code comparison. The reactivity difference is shown in Eq. (3). The power comparison is generally expressed in terms of relative difference, as shown in Eq. (4). The relative root-mean-square (RMS) disparity can then be determined using the local power differences, as shown in Eq. (5),

$$\Delta\rho(pcm) = \left(\frac{1}{k_{\text{eff}}} - \frac{1}{k_{\text{eff,reference}}}\right) \times 10^5, \tag{3}$$

$$\varepsilon(\%) = \left(\frac{\text{Power}}{\text{Power}_{\text{reference}}} - 1\right) \times 100\%, \tag{4}$$

$$RMS(\%) = \sqrt{\frac{\sum_{i=1}^{n} \varepsilon^2}{n}} \times 100\%, \tag{5}$$

where i represents the assembly or mesh index and n represents the total number of assemblies or meshes in a given problem. The error propagation method, in particular, is used to determine the uncertainty of the reactivity difference when calculating the FTC and CTC.

Table 5
Summary of core TH parameters for different flow rate distributions.

Parameter	No TH1D	TH1D uniform flow rate	TH1D zone-wise flow rate
k_{eff}	1.00940	1.00983	1.00982
Average fuel temperature (K)	750	714.4	714.8
Max. fuel centerline temperature (K)	–	837.9	816.7
Average coolant temperature (K)	648.15	648.2	648.6
Max. coolant temperature (K)	–	761.9	752.5

Table 2 summarizes the k_{eff} from 3D whole-core ANTS-100e calculations using MCS/RF and MCS at the beginning of the cycle at ARO. The eigenvalue discrepancy was found to be less than 77 pcm, indicating that the results obtained from the MCS/RF code agree with those obtained from the reference MCS code. In addition, Fig. 8 depicts the MCS/RF radial power distribution and its local relative difference to the reference MCS results, whereas Fig. 9 depicts the MCS/RF and MCS axial power profiles. Table 3 summarizes the maximum and RMS relative differences in radial and axial power. The results demonstrate that the RMS and maximum relative differences in radial power are less than 0.39% and 0.77%, respectively, which also indicates a good agreement between the two codes. The considerable axial power differences can be seen at the core top and bottom, where the local powers are low. A further analysis of the reactivity coefficients (the FTC and CTC in Table 2) obtained by MCS/RF reveals excellent agreement with MCS, with relative differences falling within three SDs. Notably, the CTC relative SDs are quite significant. This can be attributed to the small change in LBE density even when the temperature changes significantly, resulting in a small reactivity difference.

Table 4 displays the control rod worths (CRWs) computed by MCS and MCS/RF. Because no correction is applied, RF overestimates the impact of the CRAs at all rods in (ARI) by approximately 5.8% for ANTS-100e. When the SPH factor is used only in the control rod region, the

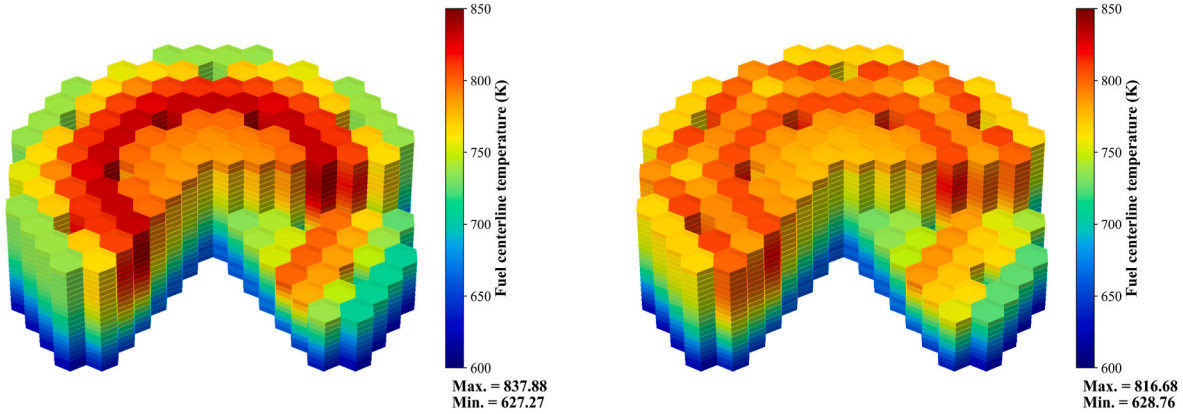

Fig. 11. Fuel centerline temperature distribution, uniform flow rate (left) vs. zone-wise flow rate (right).

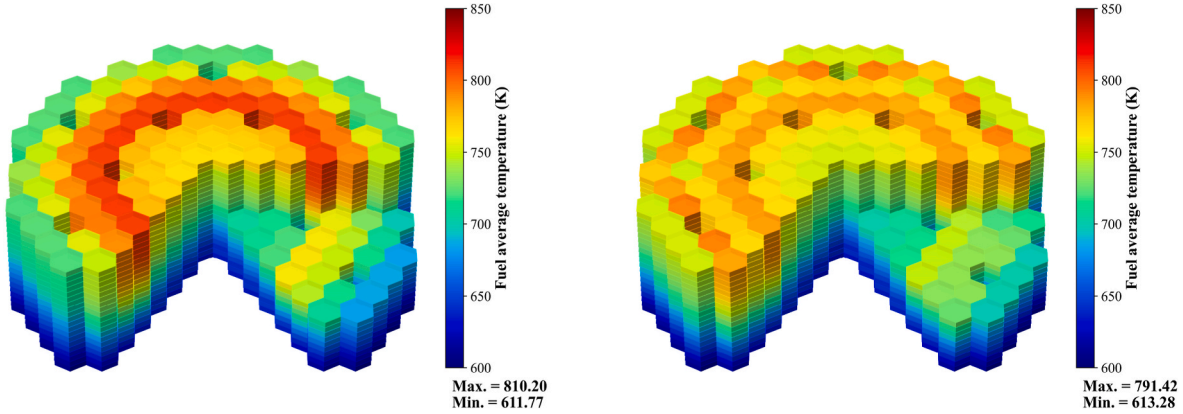

Fig. 12. Fuel average temperature distribution, uniform flow rate (left) vs. zone-wise flow rate (right).

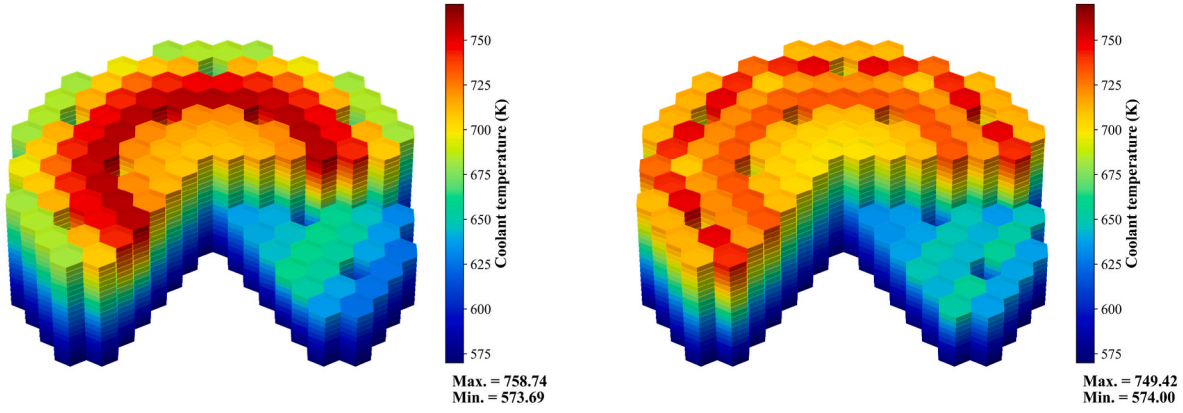

Fig. 13. Coolant temperature distribution, uniform flow rate (left) vs. zone-wise flow rate (right).

results improve, but the CRW difference remains significant, nearly 2.0%. Once the SPH-corrected XSs are used for both the CRA and its surrounding FAs, the RF solutions appear to yield to the MCS rod worth when the difference is approximately 0.2%. The control rod XS is primarily responsible for the difference, and further improvement is achieved once the adjustment is applied to its surroundings. Because the assembly pitch is quite large, which is almost identical to the neutron mean free path in fast reactors, the SPH factor is only applied to six-surrounding FAs. Furthermore, RF has the capability of automatically adjusting the XS of the CRA and its surrounding FAs by the corresponding SPH factors when rodded at a specific point. This function is useful when inserting or removing the CRA in stages for transient analysis.

4.2. *Neutronic simulation with TH1D feedback*

Several parameters are introduced to provide a summary of the TH simulation. The average linear heat generation over the core is 12.86 kW/m, and the local peak linear heat generation in the hottest assembly is approximately 16.33 kW/m. Each channel has 20 axial meshes (5 cm per mesh). The coolant is assumed to have an inlet temperature of 573.15 K and a pressure of 0.1 MPa. The flow orifices have been installed

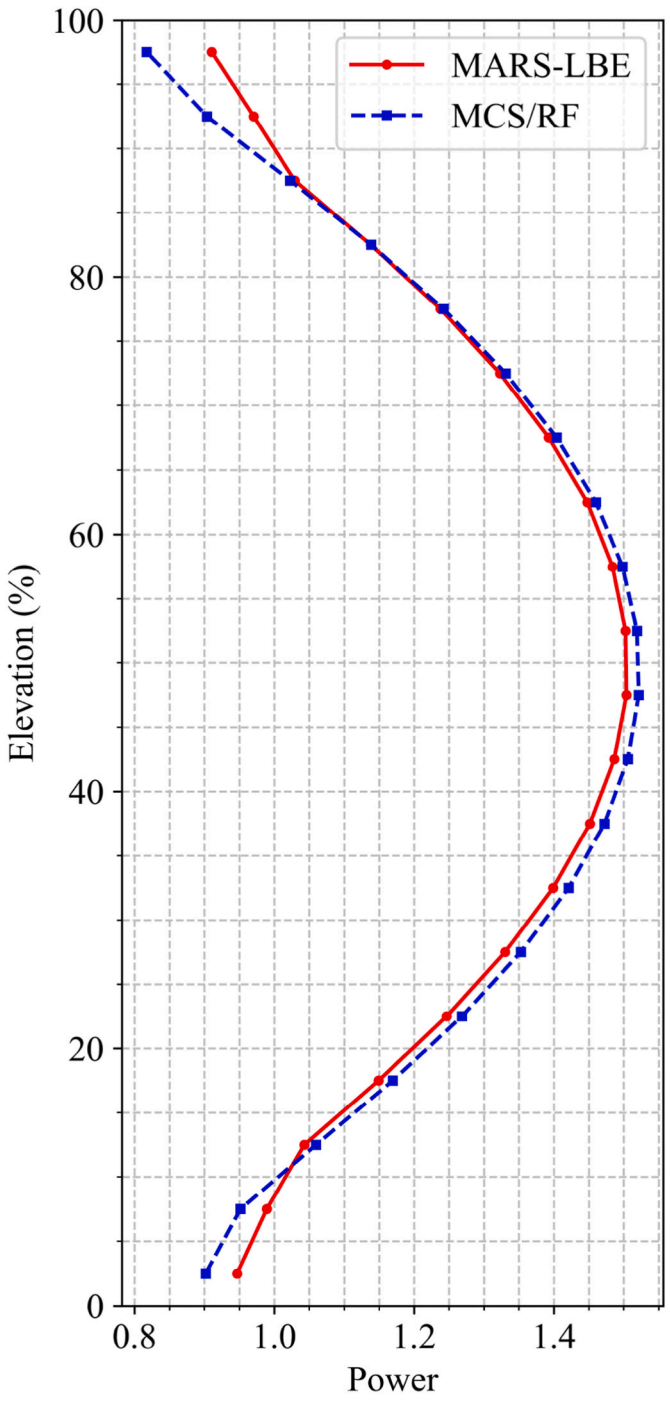

Fig. 14. Axial power used in MCS/RF and MARS-LBE at hottest assembly.

to regulate the channel flow rate, and three distinct flow zones (as shown in Fig. 10, suggested by Kim et al. [27]) are used to flatten the outlet coolant and fuel temperatures. To achieve an outlet coolant temperature of 723.15 K and a full output power of 100 MW_e, the total flow rate is approximately 13,854 kg/s. The electric power output can be regulated by adjusting the core flow rate with the maximum electric power of 100MW_e as specified. The average and maximum velocity of the coolant are 0.97 m/s and 1.12 m/s, respectively.

Two simulations are conducted: the first one uses a uniform flow rate of 100.39 kg/s per FA throughout the reactor, whereas the second one uses a zone-wise flow rate distribution that was suggested based on the results of prior analyses. Notably, the total flow rate in both cases remains the same. Table 5 summarizes several parameters of interest including the k_{eff}, maximum fuel centerline and average temperature, and average coolant temperature. The reactivity increases with the use of the TH1D feedback because the steady-state calculation uses the estimated average fuel temperature of 750 K. Because of the similar average fuel temperature, there is no significant difference in reactivity when using uniform or zone-wise flow rate. However, using the zone-wise flow rate results in a 20 K reduction in fuel centerline temperature.

Figs. 11–13 depict the 3D distribution of the fuel centerline, average temperature, and coolant temperature for the two simulations. It can be observed that the zone-wise flow rate approach leads to a more flattened temperature distribution compared to the uniform flow rate approach. As mentioned, the zone-wise flow rate approach results in a reduction in the peak fuel temperature, which can improve the safety and reliability of the reactor. This analysis confirms the importance of considering a channel-wise flow rate approach in the design and operation of LMFRs. By optimizing the flow rate distribution, it is possible to achieve a more uniform temperature distribution and improve the performance of the reactor.

To verify the accuracy of the MCS/RF simulation with TH1D feedback, an additional TH analysis is performed for the ANTS-100e core based on the MCS radial and axial power using the MARS-LBE code system [27]. MARS-LBE is a 1D system TH code that has been developed from the MARS 3.1 release and specializes in applications on LMFR systems [28]. In this analysis, the core is considered to have three main domains (in addition to three hottest assemblies for each domain) corresponding to the zone-wise flow rate. In total, there are 6 zones, and the core average axial power spectrum is applied to all specified zones. On the other hand, each FA is treated as a single TH channel and the local mesh-dependent power is employed in RF. Fig. 14 shows the axial power used in the hottest assembly in MCS/RF and MARS-LBE.

Figs. 15 and 16 compare the axial fuel centerline temperature, cladding temperature, and coolant temperature of MCS/RF and MARS-LBE, in which the relative difference in temperature is defined in Eq. (6).

$$\text{Rel. Diff. } (\%) = \left(\frac{T_{\text{MCS/RF}}}{T_{\text{MARS-LBE}}} - 1 \right) \times 100\%. \tag{6}$$

It can be seen that the difference in fuel centerline temperature at the hottest assembly follows the difference in axial power in Fig. 14, with the MCS/RF predicting a lower fuel temperature at the top and bottom of the core and a higher fuel temperature at the core center. Nevertheless, a code-to-code comparison shows good agreement, with relative differences of less than 0.8%, despite differences in simulation parameters and the use of different approaches to calculate the linear heat applied by each channel. This demonstrates the accuracy and reliability of the MCS/RF simulation with TH1D feedback in capturing the TH behavior of the ANTS-100e core.

It is worth noting that the comparison between MCS/RF and MARS-LBE serves as a benchmark test for the validation of the two-step code system. In fact, the consistent verification of RF against MARS-LBE requires the use of the converged RF power profiles from the coupled RF/TH1D iterations instead of MCS power profiles. However, it should be noted that the RF power profiles agree accurately with the MCS standalone simulations. Secondly, the RF/TH1D power profiles do not deviate significantly from the steady-state simulation. As a result, despite several differences in approach mentioned in the manuscript, there is good agreement between those results. Nevertheless, the results of this test provide confidence in the ability of the MCS/RF simulation to accurately model the TH feedback in LMFRs. The excellent agreement between the two code systems also indicates that the approach used in MCS/RF coupled with TH1D is a valid approximation that can provide accurate results. More studies should be conducted for SFRs to further verify the MCS/RF capability in simulation with TH feedback.

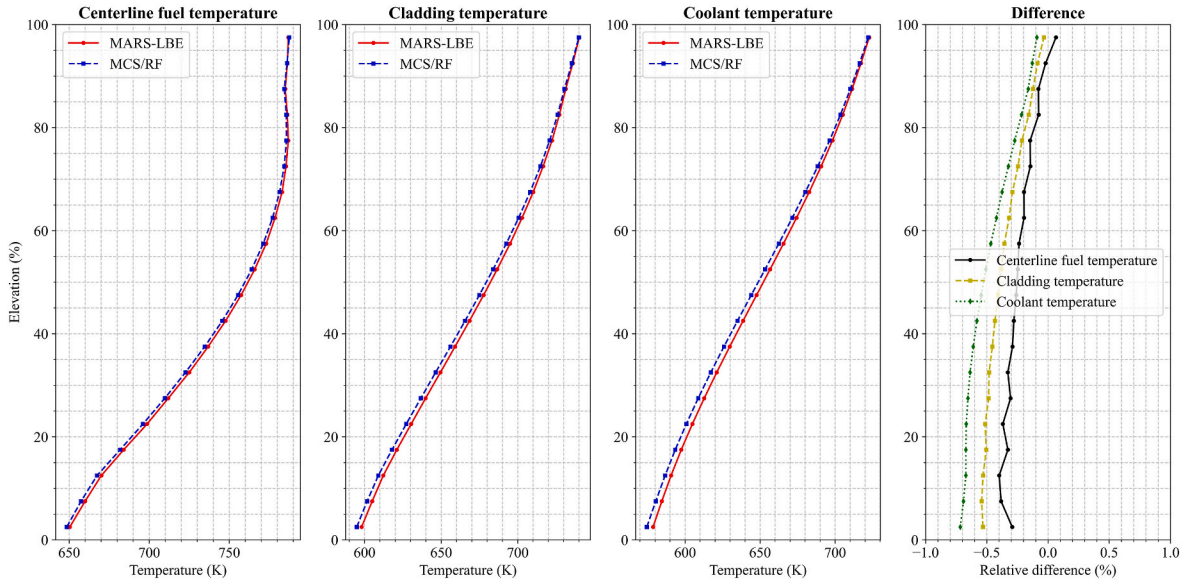

Fig. 15. Core average axial temperature distribution comparison, MCS/RF vs. MARS-LBE.

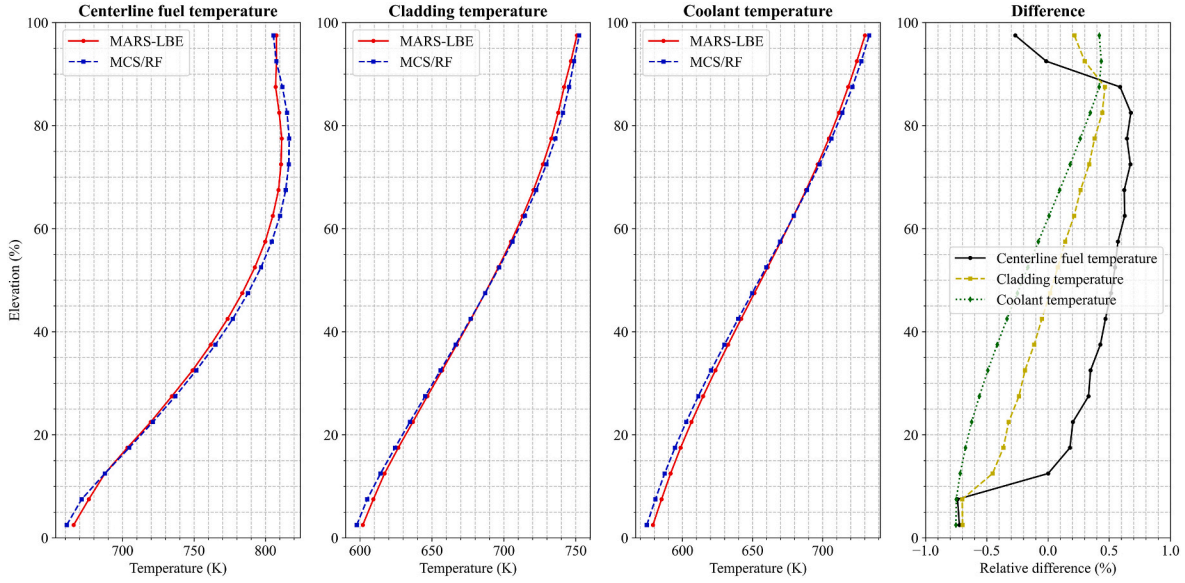

Fig. 16. Axial temperature distribution comparison at hottest assembly, MCS/RF vs. MARS-LBE.

5. Conclusions

In this study, the use of the MCS MC code for MG XS generation in nodal diffusion simulator-based FR simulations was investigated, and the procedure was validated through core steady-state neutronic calculation and neutronic coupled with TH1D simulation. The results demonstrate that the MCS/RF code system is capable of generating accurate MG XSs for the FR whole-core study. The k_{eff} difference between MCS/RF and MCS is less than 77 pcm, and the RMS differences in radial and axial power are less than 0.5% and 0.25%, respectively. Furthermore, the reactivity feedback coefficients (the FTC and CTC) determined by MCS/RF agree with those obtained by MCS. The verification of the MCS/RF coupled with TH1D simulation for ANTS-100e using the case matrix obtained by MCS branch calculations revealed significant agreement with the relative differences in fuel and coolant temperature of less than 0.8%. In summary, this study demonstrates that the MCS/RF code system with TH1D feedback is a viable approach for LMFR simulations.

This study has several limitations that necessitate additional research and development, which could lead to improved accuracy and efficiency in FR analysis and, eventually, contribute to the design and operation of more sustainable nuclear reactors. The research only considers steady-state simulations and feedback from fuel and coolant temperatures. Future research ought to investigate the depletion calculation with TH feedback in addition to axial and radial expansion. Furthermore, the effect of XS uncertainties from the selected library on simulation accuracy is not addressed in this study. Another limitation is the inconsistency in the TH modeling between RF/TH1D and MARS-LBE. More references, such as the implementation of coupling scheme MCS/TH1D for FRs, should be produced to verify the RF/TH1D. A comprehensive uncertainty analysis, including sensitivity and uncertainty quantification studies, might strengthen our understanding of the key factors influencing reactor behavior and aid in reactor design. It would also be worthwhile to investigate the potential of artificial intelligence and machine learning techniques for improving the accuracy and efficiency of LMFR simulations.

Declaration of competing interest

The authors declare that they have no known competing financial interests or personal relationships that could have appeared to influence the work reported in this paper.

Acknowledgments

This work was partially supported by the National Research Foundation of Korea (NRF) grant funded by the Korea government (MSIT) (No. NRF-2019M2D2A1A03058371). This work was partially supported by Korea Institute of Energy Technology Evaluation and Planning (KETEP) grant funded by the Korea government (MOTIE) (RS-2023-00241302).

References

[1] E. Fridman, E. Nikitin, A. Ponomarev, A. Di Nora, S. Kliem, K. Mikityuk, Extension of the DYN3D/ATHLET code system to SFR applications: models description and initial validation, Ann. Nucl. Energy 182 (2023), 109619.
[2] W.C. Dawn, S. Palmtag, A multiphysics simulation suite for liquid metal-cooled fast reactors, Ann. Nucl. Energy 159 (2021), 108213.
[3] B. Lindley, et al., Impact of thermal-hydraulic feedback and differential thermal expansion on European sodium-cooled fast reactor core power distribution, J. Nucl. Eng. Radiat. Sci. 9 (2023), 031301.
[4] M. Vazquez, H. Tsige-Tamirat, L. Ammirabile, F. Martin-Fuertes, Coupled neutronics thermal-hydraulics analysis using Monte Carlo and sub-channel codes, Nucl. Eng. Des. 250 (2012) 403–411.
[5] C. Fang, et al., Neutronics and thermal-hydraulics coupling analysis for a small lead-based fast reactor based on the discrete ordinate nodal and parallel channel method, Front. Energy Res. 11 (2023), 1088718.
[6] T.D.C. Nguyen, D. Lee, Group constants generation by Monte Carlo code MCS for LWR analysis, Comput. Phys. Commun. 285 (2023), 108642.
[7] T.D.C. Nguyen, H. Lee, D. Lee, Use of Monte Carlo code MCS for multigroup cross section generation for fast reactor analysis, Nucl. Eng. Technol. 53 (2021) 2788–2802.
[8] J. Park, et al., RAST-K v2—three-dimensional nodal diffusion code for pressurized water reactor core analysis, Energies 13 (2020) 6324.
[9] T.Q. Tran, A. Cherezov, X. Du, D. Lee, Verification of a two-step code system MCS/RAST-F to fast reactor core analysis, Nucl. Eng. Technol. 54 (2022) 1789–1803.
[10] T.D.C. Nguyen, J.Y. Kim, J. Choe, I.C. Bang, D. Lee, Core design of 100MWe advanced nitride-fueled simplified liquid metal cooled fast reator, in: International Conference on Fast Reactors and Related Fuel Cycles: Sustainable Clean Energy for the Future (FR22), IAEA, Vienna, Austria, 2022. April 19-22 2022.
[11] H. Lee, et al., MCS–A Monte Carlo particle transport code for large-scale power reactor analysis, Ann. Nucl. Energy 139 (2020), 107276.
[12] V. Dos, H. Lee, J. Choe, H.C. Shin, H.S. Lee, D. Lee, Validation of UNIST MCS Monte Carlo code system for OPR-1000, in: Korean Nuclear Society Spring Meeting, Jeju, Korea, Korean Nuclear Society, May .
[13] V. Dos, H. Lee, X. Du, D. Lee, MCS analysis of 1000 MWth sodium-cooled fast reactor, in: International Congress on Advances in Nuclear Power Plants, France, Juan-Les-Pins, French Nuclear Society, May .
[14] T.D.C. Nguyen, H. Lee, S. Choi, D. Lee, Validation of UNIST Monte Carlo code MCS using VERA progression problems, Nucl. Eng. Technol. 52 (2020) 878–888.
[15] T.D.C. Nguyen, H. Lee, S. Choi, D. Lee, MCS/TH1D analysis of VERA whole-core multi-cycle depletion problems, Ann. Nucl. Energy 139 (2020), 107271.
[16] J. Choe, et al., Verification and validation of STREAM/RAST-K for PWR analysis, Nucl. Eng. Technol. 51 (2019) 356–368.
[17] E. Fridman, J. Leppänen, On the use of the Serpent Monte Carlo code for few-group cross section generation, Ann. Nucl. Energy 38 (2011) 1399–1405.
[18] E. Fridman, E. Shwageraus, Modeling of SFR cores with Serpent–DYN3D codes sequence, Ann. Nucl. Energy 53 (2013) 354–363.
[19] E. Nikitin, E. Fridman, K. Mikityuk, On the use of the SPH method in nodal diffusion analyses of SFR cores, Ann. Nucl. Energy 85 (2015) 544–551.
[20] H. Lee, Development of a New Monte Carlo Code for Large-Scale Power Reactor Analysis, Doctorate, Nuclear Engineering, Ulsan National Institute of Science and Technology, 2019.
[21] V. Bobkov, L. Fokin, E. Petrov, V. Popov, V. Rumiantsev, A. Savvatimsky, Thermophysical Properties of Materials for Nuclear Engineering: a Tutorial and Collection of Data, IAEA, Vienna, 2008.
[22] C. Fazio, et al., Handbook on Lead-Bismuth Eutectic Alloy and Lead Properties, Materials Compatibility, Thermal-Hydraulics and Technologies-2015 Edition, Organisation for Economic Co-Operation and Development, 2015.
[23] Challenges Related to the Use of Liquid Metal and Molten Salt Coolants in Advanced Reactors, Report of the collaborative project COOL of the international project on innovative nuclear reactors and fuel cycles (INPRO), IAEA (May 15 2013). IAEA-TECDOC-1696.
[24] G.J. Calamai, et al., Steady State Thermal and Hydraulic Characteristics of the FFTF Fuel Assemblies, June 1974. FRT-1582.
[25] S. Cevolani, E. Nava, K.W. Burn, Power Deposition Distribution In Liquid Lead Cooled Fission Reactors And Effects On The Reactor Thermal Behaviour, Ente Per Le Nuove Tecnologia 33, Italy, 2001, p. 16. ENEA-RT-ERG–01-04.
[26] H. Guo, X. Huo, K. Feng, H. Gu, Verification of OpenMC for fast reactor physics analysis with China experimental fast reactor start-up tests, Nucl. Eng. Technol. 54 (2022) 3897–3908.
[27] J.Y. Kim, T.D.C. Nguyen, D. Lee, I.C. Bang, Preliminary safety analysis results of lead cooled fast reactor design using MARS code, in: Korean Nuclear Society Virtual Autumn Meeting, Korean Nuclear Society, 2020, pp. 17–18. December.
[28] B.D. Chung, et al., MARS Code Manual Volume I: Code Structure, System Models, and Solution Methods, KAERI/TR–2812/2004 42, Korea Atomic Energy Research Institute, 2010. issue 9.